INTERNATIONAL JOURNAL FOR NUMERICAL METHODS IN ENGINEERING, VOL. 7, 255–271 (1973)

NON-LINEAR TRANSIENT FINITE ELEMENT ANALYSIS WITH CONVECTED CO-ORDINATES

T. BELYTSCHKO† AND B. J. HSIEH‡
University of Illinois at Chicago Circle, Chicago, Illinois, U.S.A.

SUMMARY

A finite element method is presented for the transient analysis of large-displacement, small-strain problems with material non-linearities. The method employs a convected co-ordinate technique and a direct nodal force computational scheme of considerable efficiency. Detailed formulations are given for a plane, constant strain triangular element and a Euler–Bernoulli beam element. Results are presented for several example problems and compared with experimental data and other numerical solutions.

INTRODUCTION

Because of the inordinately taxing computational requirements of transient non-linear analysis, an efficient formulation is imperative if large scale problems are to be undertaken. In contrast to static analysis, where little advantage is usually gained by improvements in the procedure for stiffness calculations, such efficiencies in dynamic problems are of major importance. Hence the computational improvement of dynamic schemes in both the integration and nodal force computations has recently attracted the attention of several investigators.[1–3]

The finite element method was first applied to transient dynamic analysis by Costantino,[4] who treated problems linear in both materials and geometry. Subsequent development of non-linear transient techniques closely paralleled the development of the static displacement method. Costantino[5] applied the finite element method to dynamic problems with non-linear materials by using a fictitious (or pseudo) force approach, similar to a technique first employed by Gallagher and co-workers[6] in static analysis. Tangential stiffness methods were applied to dynamic problems with non-linear materials by Dibaj and Penzien[7] and Farhoomand and Wilson.[8]

The first departure from stiffness matrix formulations appears to be Oden,[9,10] who formulated the dynamic transient problem including both geometric and material non-linearities by expressing nodal forces directly in terms of stresses. Similar formulations have also been reported by Malone and Connors[11] (without geometric non-linearities), Wu and Witmer[12] and Hartzman and Hutchinson.[13] A tangential stiffness method for problems with geometric and material non-linearities has been developed by Stricklin and co-workers[1] and by McNamara and Marcal.[14] These methods are of advantage in some cases for they use implicit integration, which has no stability limitations.

In the development of geometrically non-linear programs, Lagrangian co-ordinates appear to have been preferred. All of the investigators cited in the previous paragraph used a Lagrangian description, with the exception of Hartzman and Hutchinson, who used a semi-Eulerian description. The geometric non-linearity in these analyses is treated by including the quadratic terms

† Assistant Professor of Structural Mechanics.
‡ Research Assistant.

Received 23 August 1972
Revised 18 May 1973

in the strain–displacement equations. Particularly in flexural elements, where nodal forces are computed by numerical quadrature, the evaluation of these terms requires many computations.

In this paper the computational advantages of a convected co-ordinate procedure for the large-displacement, small-strain problem are explored. Though these methods have been employed in static analyses by several investigators, among them Argyris and co-workers,[15] Wempner,[16] Murray and Wilson[17] and Levine and co-workers[18] (see Gallagher[19] for a survey), they do not appear to have been exploited in transient dynamic analysis. Yet it is for these problems that convected co-ordinates are particularly suited. If the strains are small, this formulation linearizes the strain–displacement and simplifies nodal force–stress relations within the elements' convected co-ordinates. The large displacement effects are treated entirely by transformations of displacement and force components between global and convected element co-ordinates. Hence the complexity of nodal force computations is reduced and significant improvements in computer time can be realized. Moreover, unlike Eulerian formulations, convected formulations do not complicate the constitutive laws for anisotropic materials.

The basic equations for the dynamic problem are developed in the next section. This convected co-ordinate formulation is somewhat different from the previous developments, such as that of Argyris and co-workers, in that expressions are developed for total strains and nodal forces rather than linearized increments. This may be of advantage in dynamic problems since it eliminates one source of truncation error. The third section outlines the application of this technique to a plane triangular element and a beam element. Examples are presented in the fourth section.

FORMULATION

Let the continuum or structure be subdivided into n_e discrete elements appropriately connected by nodes. The nodal displacements which pertain to a particular element I are designated as local nodal displacements $\{d\}_I$, while the set of all nodal displacements are designated as global nodal displacements $\{d\}$. The two are related by a Boolean connectivity matrix $[\mathbf{L}]_I$ (see References 10 and 15)

$$\{d\}_I = [\mathbf{L}]_I\{d\} \tag{1}$$

Each element is associated with a convected co-ordinate system $\{\hat{x}\}$ which is rotated relative to the fixed co-ordinates $\{x\}$ by the rigid body rotation of that element. If the rigid body rotation is not constant within the element, an angle which approximates the rigid body rotation is used. The displacements of each element are then subdivided into rigid body displacements $\{u^{\text{rig}}\}$ and displacements that result only in deformation $\{u^{\text{def}}\}$. Local nodal displacements can be similarly decomposed so that

$$\{d\}_I = \{d^{\text{rig}}\}_I + \{d^{\text{def}}\}_I \tag{2}$$

The displacement field in each element is represented by shape functions $[\phi]$ so that

$$\{u\} = [\phi]\{d\}_I \tag{3}$$

and it is assumed that the shape functions can represent rigid body motion, so that the deformation displacements can also be represented by

$$\{u^{\text{def}}\} = [\phi]\{\hat{d}^{\text{def}}\}_I \tag{4}$$

Displacements in convected and fixed co-ordinates are related by an orthogonal transformation

$$\{\hat{d}\}_I = [T]\{d\}_I \tag{5}$$

The stresses and strains are measured in the convected co-ordinates and denoted by $\{\hat{\sigma}\}$ and $\{\hat{\varepsilon}\}$.

It is assumed that though rotations may be arbitrarily large, the deformations themselves are small; i.e. we are considering a large displacement small-strain theory. Hence, as shown in the Appendix, the relationships between the strains and deformation displacements, $\{u^{\text{def}}\}$ in the convected co-ordinate system of each element are linear. Therefore, from equation (4) and the appropriate linear strain displacement equations, a matrix [**E**] can be derived so that

$$\{\hat{\varepsilon}\} = [\mathbf{E}]\{\hat{d}^{\text{def}}\}_I \tag{6}$$

The discrete equations are derived by the principle of virtual work, which states that the variation of the difference between internal and external work with respect to kinematically admissible displacements vanishes. This can be written as

$$\delta(W^{\text{int}} - W^{\text{ext}}) = 0 \tag{7}$$

Since both $\{\hat{\sigma}\}$ and $\{\hat{\varepsilon}\}$ are expressed in co-ordinates that rotate with the element and since deformations are small, the variation of internal work is

$$\delta W^{\text{int}} = \sum_{I=1}^{n_e} \int_{V_I} \{\delta\hat{\varepsilon}\}^{\text{T}}\{\hat{\sigma}\} \tag{8}$$

The d'Alembert inertial forces are $(-\rho\{\ddot{u}\})$, where ρ is the density and superscript dots denote time derivatives, while externally applied nodal forces are denoted by $\{F^{\text{ext}}\}$. If we include the d'Alembert forces as body forces, then

$$\delta W^{\text{ext}} = \{\delta d\}^{\text{T}}\{F^{\text{ext}}\} - \sum_{I=1}^{n_e} \int_{V_I} \rho\{\delta u\}^{\text{T}}\{\ddot{u}\} \tag{9}$$

Equations (8) and (9) are then inserted into equation (7), followed by the application of equations (3), (5) and (6), yielding

$$\sum_{I=1}^{n_e} \left(\{\delta d^{\text{def}}\}_I^{\text{T}}[T]^{\text{T}} \int_{V_I} [\mathbf{E}]^{\text{T}}\{\hat{\sigma}\} + \{\delta d\}_I^{\text{T}} \int_{V_I} \rho[\phi]^{\text{T}}[\phi]\{\ddot{d}\}_I \right) - \{\delta d\}^{\text{T}}\{F^{\text{ext}}\} = 0 \tag{10}$$

We now define local internal nodal forces by

$$\{f\}_I = [T]^{\text{T}} \int_{V_I} [\mathbf{E}]^{\text{T}}\{\hat{\sigma}\} \tag{11}$$

global internal forces by

$$\{F^{\text{int}}\} = \sum_{I=1}^{n_e} [L]_I^{\text{T}}\{f\}_I \tag{12}$$

local mass matrix by

$$[\mathbf{m}]_I = \int_{V_I} \rho[\phi]^{\text{T}}[\phi] \tag{13}$$

and global mass matrix by

$$[\mathbf{M}] = \sum_{I=1}^{n_e} [L]_I^{\text{T}}[\mathbf{m}]_I[L]_I \tag{14}$$

The operations indicated by equations (11)–(14) need not be performed explicitly; they simply represent a topologically appropriate summation of the local matrices.

Making use of the above definitions, we find

$$\sum_{I=1}^{n_e} \{\delta d^{\text{def}}\}_I^{\text{T}} \{f\}_I + \{\delta d\}^{\text{T}} [\mathbf{M}] \{\ddot{d}\} - \{\delta d\}^{\text{T}} \{F^{\text{ext}}\} = 0 \tag{15}$$

In order to extract the governing equations, we note that for a simply connected element, the local nodal forces of an element, $\{f\}_I$, must be self-equilibrated. Hence

$$\{\delta d^{\text{rig}}\}_I^{\text{T}} \{f\}_I = 0 \tag{16}$$

This is the key step in the derivation for without it the final equations cannot be derived. If equation (16) is added to the first term of equation (15), and we make use of equations (1), (2) and (12), we obtain

$$\{\delta d\}^{\text{T}} (\{F^{\text{int}}\} + [\mathbf{M}] \{\ddot{d}\} - \{F^{\text{ext}}\}) = 0 \tag{17}$$

Invoking the arbitrariness of the virtual displacements $\{\delta d\}$, we then find

$$\{\ddot{d}\} = [\mathbf{M}]^{-1} (\{F^{\text{ext}}\} - \{F^{\text{int}}\}) \tag{18}$$

where the internal nodal forces are defined by equations (11) and (12).

A flowchart of the computational procedure which implements this transient dynamic finite element scheme is shown in Figure 1. The equations of motion are here integrated explicitly in

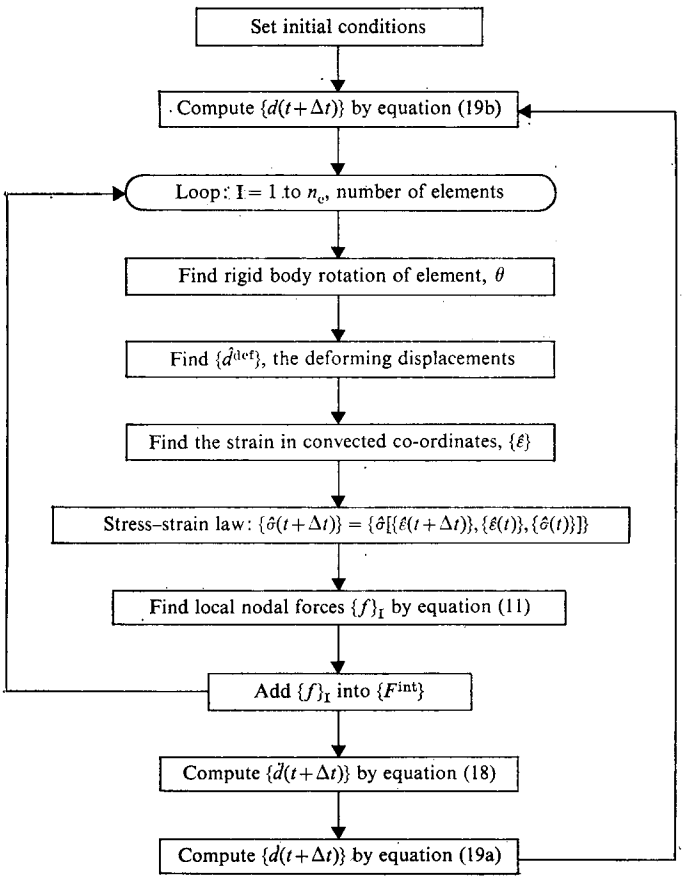

Figure 1. Flowchart of computational procedure

time by a difference method in which the velocities and displacements are computed by

$$\{\dot{d}(t+\Delta t)\} = \{\dot{d}(t)\} + \tfrac{1}{2}\Delta t[\{\ddot{d}(t)\} + (\ddot{d}(t+\Delta t)\}] \tag{19a}$$

$$\{d(t+\Delta t)\} = \{d(t)\} + \Delta t\{\dot{d}(t)\} + \tfrac{1}{2}\Delta t^2\{\ddot{d}(t)\} \tag{19b}$$

The convective co-ordinate formulation can however be used with any explicit integration scheme.

As can be seen from the flowchart, the procedure is applicable to arbitrary non-linear materials. A stress–strain law of the form

$$\{\hat{\sigma}(t+\Delta t)\} = \{\hat{\sigma}[\{\hat{\varepsilon}(t+\Delta t)\}, \{\hat{\varepsilon}(t)\}, \{\hat{\sigma}(t)\}]\} \tag{20}$$

has been assumed here, but other state variables may easily also be included. Furthermore, since both the stress and strain are measured in the convected co-ordinates, the relationship is independent of the rigid body rotation, so stress-rate and strain-rate dependence are easily introduced.

ELEMENTS

In this section, the application of the formulation developed in the previous section is outlined for two elements:

1. A linear displacement, plane triangular element, and
2. A rectilinear Euler beam.

The elements' co-ordinate systems are shown in Figure 2.

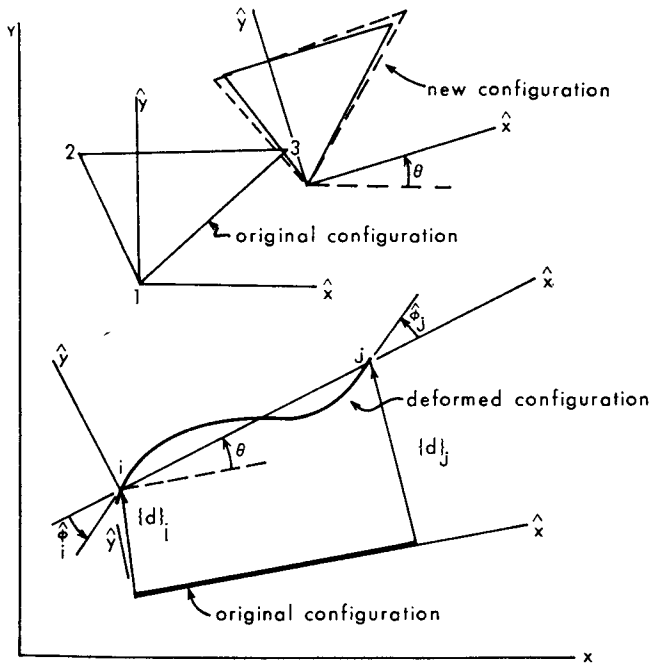

Figure 2. Elements and co-ordinates

The triangular element is the standard simplex element. The displacement field of this triangular element relative to node 1 can be written as

$$\begin{Bmatrix} u^x(\hat{x},\hat{y}) \\ u^y(\hat{x},\hat{y}) \end{Bmatrix} = \begin{bmatrix} b_{11} & b_{12} \\ b_{21} & b_{22} \end{bmatrix} \begin{Bmatrix} \hat{x} \\ \hat{y} \end{Bmatrix} \tag{21}$$

This displacement field is identical to the homogeneous deformation field used by Biot[20] in his work on incremental mechanics. From his development, it follows immediately that the angle of rigid body rotation is given by

$$\theta = \tan^{-1}\frac{b_{21}-b_{12}}{2+b_{11}+b_{22}} \tag{22}$$

which can be expressed in terms of nodal displacements by

$$\tan\theta = \frac{\hat{y}_3 D_2^y - \hat{y}_2 D_3^y + \hat{x}_3 D_2^x - \hat{x}_2 D_3^x}{4A + \hat{y}_3 D_2^x - \hat{y}_2 D_3^x - \hat{x}_3 D_2^y + \hat{x}_2 D_3^y} \tag{23}$$

where A is the area of the element and D_i are the nodal displacements relative to node 1. Once the angle of rigid body rotation is known, the corresponding rigid body displacements can be found. The deformation nodal displacements $\{D_i^{\text{def}}\}$ can then be found at each node by subtracting the rigid body displacements from the total displacements, which gives

$$\begin{Bmatrix} \hat{D}_i^{x,\text{def}} \\ \hat{D}_i^{y,\text{def}} \end{Bmatrix} = [a]\begin{Bmatrix} D_i^x \\ D_i^y \end{Bmatrix} + ([a]-[I])\begin{Bmatrix} \hat{x}_i \\ \hat{y}_i \end{Bmatrix} \tag{24}$$

where

$$[a] = \begin{bmatrix} \cos\theta & \sin\theta \\ -\sin\theta & \cos\theta \end{bmatrix} \tag{25}$$

For small strains, regardless of the size of the displacements, the strains are linearly related to the deformation displacements by

$$\left.\begin{aligned} \hat{\varepsilon}_x &= \partial\hat{u}^{x,\text{def}}/\partial\hat{x}, \quad \hat{\varepsilon}_y = \partial\hat{u}^{y,\text{def}}/\partial\hat{y} \\ 2\hat{\varepsilon}_{xy} &= \partial\hat{u}^{x,\text{def}}/\partial\hat{y} + \partial\hat{u}^{y,\text{def}}/\partial\hat{x} \end{aligned}\right\} \tag{26}$$

Since the deformation displacement field $\{\hat{u}^{\text{def}}\}$ can also be expressed in the form of equation (21), it follows that

$$\begin{Bmatrix} \hat{\varepsilon}_x \\ \hat{\varepsilon}_y \\ 2\hat{\varepsilon}_{xy} \end{Bmatrix} = \frac{1}{2A}\begin{bmatrix} \hat{y}_3 & 0 & -\hat{y}_2 & 0 \\ 0 & -\hat{x}_3 & 0 & \hat{x}_2 \\ -\hat{x}_3 & \hat{y}_3 & \hat{x}_2 & -\hat{y}_2 \end{bmatrix}\begin{Bmatrix} \hat{D}_2^{x,\text{def}} \\ \hat{D}_2^{y,\text{def}} \\ \hat{D}_3^{x,\text{def}} \\ \hat{D}_3^{y,\text{def}} \end{Bmatrix} \tag{27}$$

This equation defines the matrix [E] in equation (6); from equation (11) it follows that the nodal forces are given by

$$\begin{Bmatrix} f_2^x \\ f_2^y \\ f_3^x \\ f_3^y \end{Bmatrix} = A\begin{bmatrix} [a]^{\mathrm{T}} & [0] \\ [0] & [a]^{\mathrm{T}} \end{bmatrix}[\mathbf{E}]^{\mathrm{T}}\{\hat{\sigma}\} \tag{28}$$

Since the system of nodal forces is self-equilibrated, the nodal forces at node 1 are given by

$$f_1^x = -(f_2^x + f_3^x), \quad f_1^y = -(f_2^y + f_3^y) \tag{29}$$

A more elegant development of convected co-ordinates for simplex elements is given by Argyris and co-workers,[15] who take the deformation displacements, or degrees of flexibility, to be the elongations of the element sides. That formulation is incremental rat her than total, so the approach presented here may be preferable in transient problems. A total force and strain formulation

could be developed using the elongations of elements as the degrees of flexibility, though for anisotropic materials the angle of rotation would still need to be computed. It should also be remarked that in stiffness formulations the advantages of a convected formulation are reduced because the rigid body modes must be reintroduced by a matrix transformation in computing the element stiffness matrix. In explicit transient analysis, however, the rigid body modes only require the very simple additional computations shown in equation (29).

In the beam element, the convected $\hat{x}$-axis is taken to lie along the line joining the nodes. The transverse displacement is assumed to be cubic in $\hat{x}$, the axial displacement linear in $\hat{x}$. The rigid body rotation of the beam will of course vary along the length of the element. However, as long as the strains are small, the rotation relative to the $\hat{x}$-axis must be small, so the angle of rotation of the $\hat{x}$-axis, θ, is a good approximation to the rigid body rotation of the entire element.

The deformation displacements, i.e. flexibilities, of the element may then be taken to be $\hat{\phi}_i$, the nodal rotations relative to the $\hat{x}$-axis, and $\hat{\varepsilon}_m$, the midplane strain. A detailed development of stiffness evaluation in terms of these flexibilities may be found in Reference 15. The governing equations are therefore only outlined.

For the cubic transverse displacement field, the rotation of the cross-section is given by

$$\hat{\phi}(x) = \frac{\hat{\phi}_1}{l^2}(l^2 - 4l\hat{x} + 3\hat{x}^2) + \frac{\hat{\phi}_2}{l^2}(3\hat{x}^2 - 2l\hat{x}) \tag{30}$$

where

$$\hat{\phi}_1 = \phi_1 - \theta, \quad \hat{\phi}_2 = \phi_2 - \theta \tag{31}$$

The Euler–Bernoulli assumptions and strain–displacement equations (26), then give the axial strain

$$\hat{\varepsilon}_x(\hat{x}, \hat{y}) = \hat{\varepsilon}_m - \frac{\hat{y}}{l^2}[\hat{\phi}_1(6\hat{x} - 4l) + \hat{\phi}_2(6\hat{x} - 2l)] \tag{32}$$

Hence, from equation (11) it follows that the nodal forces corresponding to deformation displacements for a beam of cross-sectional area A_c are given by

$$\begin{Bmatrix} m_1 \\ m_2 \end{Bmatrix} = -\frac{1}{l^2}\int_0^l \int_{A_c} \begin{bmatrix} 6\hat{x} - 4l \\ 6\hat{x} - 2l \end{bmatrix} \hat{y}\hat{\sigma}_x(\hat{x}, \hat{y})\, dA\, d\hat{x} \tag{33}$$

$$\hat{f}_2^x = -\hat{f}_1^x = \frac{1}{l}\int_0^l \int_{A_c} \hat{\sigma}_x(\hat{x}, \hat{y})\, dA\, d\hat{x} \tag{34}$$

These integrals must be evaluated numerically. The transverse forces can be found from equilibrium to be

$$\hat{f}_1^y = -\hat{f}_2^y = \frac{m_1 + m_2}{l} \tag{35}$$

Flowcharts of the computational procedures are given in Figures 3 and 4.

In computing the midplane strain, $\hat{\varepsilon}_m$, and the angle of rotation, care must be taken to use formulae that do not result in excessive round-off errors when these variables or the displacements are small. For example

$$\hat{\varepsilon}_m = \frac{l^{new} - l^o}{l^o} \tag{36}$$

where l^o and l^{new} are the old and new lengths of the element. Direct use of these formulae will result in large round-off errors. An alternative formula can be derived by noting that if the

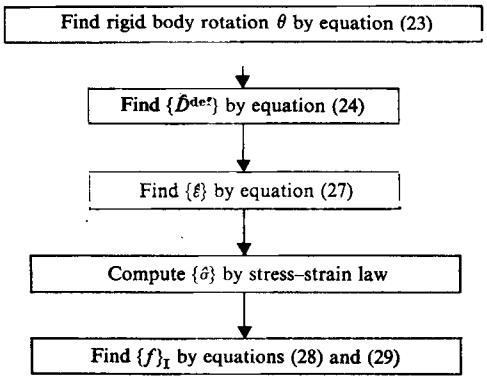

Figure 3. Flowchart of local nodal force computation for a triangular, plane element

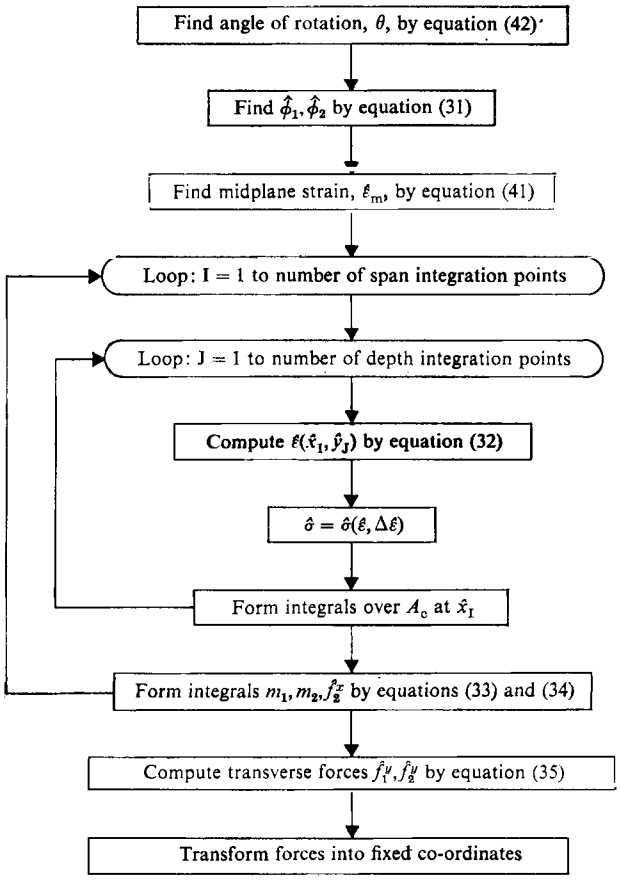

Figure 4. Flowchart of local nodal force computation for a beam element

displacements and elements are considered to be vectors, then

$$\{\mathbf{x}\}_2^{\text{new}} - \{\mathbf{x}\}_1^{\text{new}} = \{\mathbf{x}\}_2^{\text{o}} - \{\mathbf{x}\}_1^{\text{o}} + \{\mathbf{d}\}_2 - \{\mathbf{d}\}_1 \tag{37}$$

Taking the scalar product of each side of the equation with itself, it follows that

$$(l^{\text{new}})^2 = (l^{\text{o}})^2 + 2\{\mathbf{x}\}_{21} \cdot \{\mathbf{d}\}_{21} + \{\mathbf{d}\}_{21} \cdot \{\mathbf{d}\}_{21} \tag{38}$$

where

$$\{\mathbf{d}\}_{21} = \{\mathbf{d}\}_2 - \{\mathbf{d}\}_1, \quad \text{etc.} \tag{39}$$

By shifting the first term on the right-hand side to the left-hand side and factoring the resulting left-hand side, it follows that

$$l^{\text{new}} - l^{\text{o}} = \frac{1}{l^{\text{new}} + l^{\text{o}}} [2\{\mathbf{x}^{\text{o}}\}_{21} \cdot \{\mathbf{d}\}_{21} + \{\mathbf{d}\}_{21} \cdot \{\mathbf{d}\}_{21}] \tag{40}$$

hence

$$\varepsilon_{\text{m}} = \frac{1}{l^{\text{o}}(l^{\text{new}} + l^{\text{o}})} [2x_{21} d_{21}^x + 2y_{21} d_{21}^y + (d_{21}^x)^2 + (d_{21}^y)^2] \tag{41}$$

Similarly, by considering vector products it can be shown that the approximate angle of rigid body rotation, θ, is given by

$$\sin \theta = (d_{21}^y x_{21} - d_{21}^x y_{21})/(l^{\text{o}} l^{\text{new}}) \tag{42}$$

In small strain analysis, l^{o} and l^{new} need not be distinguished.

RESULTS

The convected co-ordinate method described in the previous section has been coded in a computer program called WHAM (Waves in Hysteric Arbitrary Media). A lumped, diagonal mass matrix is used. For the triangular elements, the element lumped mass matrix is formed by apportioning one-third of the mass of the element to each node. The lumped masses for the beam are assigned as follows. Each beam is divided into two segments by its midpoint; each node is then ascribed a rotational inertia equal to the mass moment of the adjacent half segment about the node and a translational inertia equal to the mass of the segment. The nodal forces for the beam, equations (33) and (34), are found by Gaussian quadrature using five points through the depth and two points along its length.

Results for three examples are presented here. For two of the examples, experimental and finite element results have been reported by Balmer and Witmer[21] and Wu and Witmer,[12] respectively.

The beam material has a Young's modulus of $1{\cdot}04 \times 10^7$ lb/in^2, a Poisson's ratio of 0·3, density of $2{\cdot}61 \times 10^{-4}$ slugs/in^3 and a yield stress $\sigma_0 = 42{,}800$ lb/in^2. An ultimate stress of 50,000 lb/in^2 is assumed. Between the yield stress and the ultimate stress, linear, isotropic hardening with a plastic modulus $E_{\text{p}} = 78{,}700$ lb/in^2 is used. Once the material attains the ultimate stress, it is taken to behave as an elastic, perfectly–plastic material. No strain rate effects are included. The beams are 1·2 in wide and 0·125 in deep, so they are essentially in a state of plane strain. Because the beam elements used here treat the state of stress as uniaxial, an exact treatment of plane strain in the plastic range is not possible with these elements; in the elastic range the transverse stress $\hat{\sigma}_t$ is given by $\nu\hat{\sigma}_x$, but if we use the von Mises criterion in the plastic range, the transverse stress varies with time and tends to $\frac{1}{2}\hat{\sigma}_x$ as the plastic strains become predominant. Therefore, an exact treatment of plane strain would require storing the transverse stresses, which is quite undesirable for larger problems. Instead an approximate treatment of plane strain was developed

as follows. Before the onset of initial yielding, $\hat{\sigma}_t = \nu\hat{\sigma}_x$ so the von Mises yield criterion given

$$\hat{\sigma}_x^2 - \nu\hat{\sigma}_x^2 + \nu^2\hat{\sigma}_x^2 \leqslant \sigma_0^2 \tag{43}$$

which gives the following yield condition

$$\hat{\sigma}_x^2 \leqslant \frac{\sigma_0^2}{1-\nu+\nu^2} \tag{44}$$

The plastic modulus is also modified for plane strain by assuming the von Mises flow law and the predominance of plastic strains, which gives

$$E_p' = \tfrac{3}{2}E_p \tag{45}$$

The first problem is a clamped beam impulsively loaded with a velocity of 5,200 in/sec over a centre segment as shown in Figure 5. The beam is subdivided into 10 elements and a time-step of 1 μsec is used, as in Reference 12. The central deflection response is shown in Figure 5 along

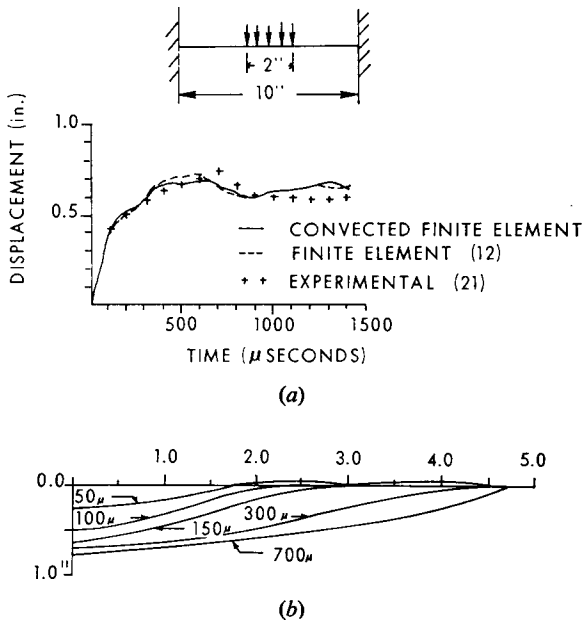

Figure 5. Central deflection and deflected shapes of an impulsively loaded, clamped beam compared to experimental results of Balmer and Witmer[21] and numerical results of Wu and Witmer[12]

with experimental results of Balmer and Witmer[21] and finite element results of Wu and Witmer.[12] Both finite element solutions compare well with the experimental results. Deflection patterns at various times are also shown in Figure 5. Maximum midplane strains in this problem, which occurred at the centre, were about 3 per cent, but most midplane strains remained below 1 per cent, so the small strain assumption is valid.

The second problem is a clamped ring impulsively loaded with a velocity of 4,862 in/sec as shown in Figure 6. The beam is subdivided into 16 rectilinear elements and a time-step of 1 μsec is used; 19 curved elements were used in Reference 12. Comparisons of the central deflection response with experimental results and previous finite difference and finite element solutions are made in Figure 6.

The maximum midplane strains in the ring are of the order of 5 per cent, so the small strain assumption is not completely valid. Since the principal directions of the stress do not change, the major effect of the large strains is the change in cross-sectional area due to the incompressibility of the plastic behaviour. This was accounted for by modifying the depth of the beam for equation (33) by

$$h = h_0(1-\varepsilon_m) \tag{46}$$

where h_0 is the original depth of the beam. This modification does not account for the effects of the variation of cross-sectional areas in sublayers of the beam due to bending nor the compressibility of the elastic strains. However, the net change in cross-sectional area due to bending in Euler–Bernoulli beam theory is zero, so equation (46) probably is an adequate reflection of the effects of incompressibility.

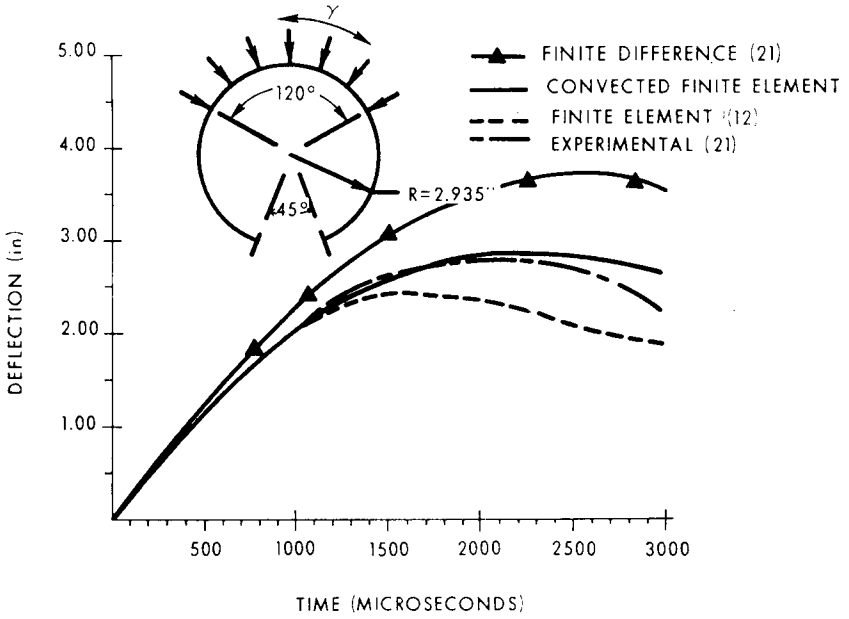

Figure 6. Central deflection results for an impulsively loaded ring compared to experimental results of Balmer and Witmer[21] and numerical results of Wu and Witmer[12]

It can be seen that the finite element results obtained here match the experimental results quite well. The computed displacements are only a little above the experimental results, so since the inclusion of any strain-rate effects would undoubtedly reduce the computed displacements, the results appear reasonable. The effects of the plane strain and incompressibility corrections were checked; it was found that including plane strain reduced the maximum displacement by 20 per cent, incompressibility by about 5 per cent. The latter was the same order as the maximum midplane strain. When neither correction was included the results closely matched the finite difference results of Reference 21.

Figures 7 and 8 show a comparison of the deflected shapes and selected strain histories with experimental results. The computed strains are not entirely satisfactory, but as can be seen from Figure 7, the strains were recorded in segments of the beam where maximum discrepancies in the deformed shape occurred.

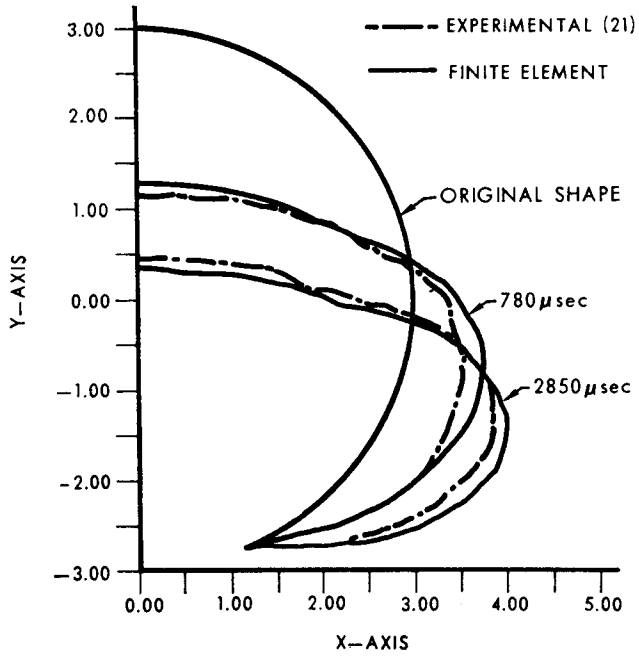

Figure 7. Deflection patterns for a ring compared to experimental results of Balmer and Witmer[21]

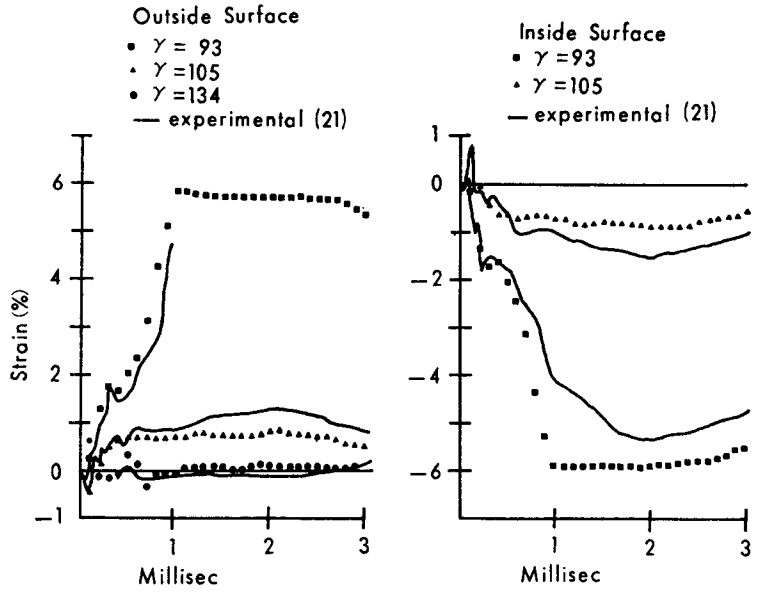

Figure 8. Strain histories for a ring compared to experimental results of Balmer and Witmer[21]

Two possible sources of error in this solution are the use of rectilinear beam elements to represent a curved beam and the use of lumped masses. The solution was therefore repeated for a 1,000 μsec run with (a) twice as many elements and (b) a consistent mass matrix. The finer mesh yielded insignificant differences in the displacement response, while the consistent mass results differed by 10 per cent or less.

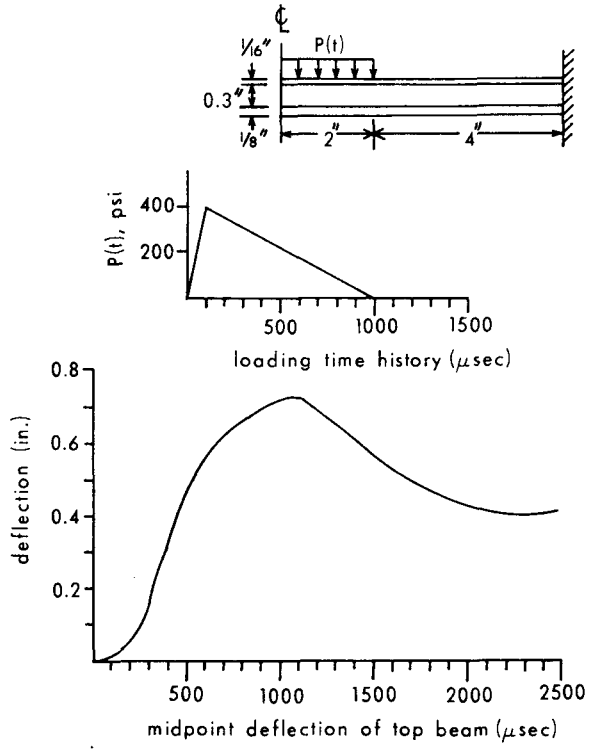

Figure 9. Central deflection of a beam for beam–fluid composite

Figure 9 shows the computed response of two beams enclosing an inviscid, compressible fluid, with a bulk modulus of 588,000 lb/in^2 and a density of $7{\cdot}72 \times 10^{-5}$ lb-sec^2/in^4. The fluid was modelled by triangular continuum elements with nodes rigidly linked to the beam node; 20 beam elements and 20 continuum elements were used to model half of the structure.

DISCUSSION

The first two problems reported here required less than two minutes of CPU time on an IBM 370/155 time sharing environment (approximately fifteen seconds on a CDC 7600) for 3,000 time-steps. Estimated element time-steps per second is 300 for the beam element, 600 for the triangular element on the IBM computer and 1,800 and 7,200 for the CDC computer, respectively. The method is bandwidth independent, so the computation times would scale up linearly for larger meshes.

It might be remarked that in addition to streamlining the computational procedure, the convected co-ordinate formulation simplifies the implementation of complex stress–strain laws. For example, the standard Lagrangian formulation of plasticity entails the use of the Jaumann

derivative for the stress rate. In the convected formulation, because of the rotation of the co-ordinate system with the element, the stress rate corresponds to simply the time derivative of $\{\hat{\sigma}\}$.

Another aspect of this convected formulation is the use of self-equilibration to compute nodal forces associated with rigid body modes. This is not only advantageous from the viewpoint of computational efficiency, but appears to benefit the accuracy and stability of the solution. It was found through a programming error that even a small (approximately 1 per cent) discrepancy in element equilibrium can cause spurious generation of energy, which results in fictitious oscillations and divergence of the solution. The need for scrupulously maintaining conservation of energy is quite obvious in view of the fact that several thousand time-steps are required in these solutions.

In conclusion, the main advantages of the convected co-ordinate description presented here are its simplicity and computational efficiency. These advantages depend on the type of element used. For simplex elements, small, if any, benefits are realized because the element stresses and strains are constant, so only a single strain and stress computation is needed to find the nodal forces. Transformation into and out of the convected co-ordinates requires as much computer time as the non-linear computations needed in the Lagrangian method. On the other hand, in flexural elements, many stress and strain calculations are required in each element, so transforming into the convected co-ordinates so that linear relationships can be employed yields substantial savings.

In addition, the use of convected co-ordinates simplifies the treatment of flexural elements with displacement components expanded in polynomials of different orders, such as cubic transverse displacements and linear axial displacements. Since the deformation displacements are separated from the rigid body motion in the convected formulation, the cubic displacement field is always normal to the midplane. In Lagrangian formulations, however, as the element rotates a portion of the transverse displacement becomes axial. Thus, if the element rotates 90°, the linear displacement field will be normal to the midplane in the final configuration, the cubic displacement field along the axis.

The development of efficient formulations for transient problems is of key importance. Whereas the major computational effort in static problems is in the solution of algebraic equations, in non-linear transient problems, strain and nodal force computations require most of the computer time. Therefore, the efficiency of these computations determines the speed of the computer code and sets the limits on the size of finite element models which are economically feasible.

ACKNOWLEDGEMENT

The support of the National Science Foundation under Grant GK 5834 is gratefully acknowledged.

APPENDIX

This Appendix deals with two aspects of the convected co-ordinate formulation: the linearity of the strain–displacement equations within the convected co-ordinates and the manner in which the well-known role of the initial stresses appear in the equations of motion, equations (11) and (18). For purposes of establishing the linearity of the strain–displacement equations for small strain–large rotation problems, we begin with the polar decomposition theorem. This theorem states that any deformation can be decomposed into a pure deformation, characterized by a symmetric transformation $(\delta_{ij}+\alpha_{ij})$, where δ_{ij} is the Kronecker delta, and a pure rotation, characterized by an orthogonal transformation a_{ij}. If the strains are small, the terms of the symmetric matrix α_{ij} are small. Let $X_i, x_i, \hat{x}_i$ be the Lagrangian, Eulerian and convected

co-ordinates, respectively. The pure deformation relates the convected and Lagrangian co-ordinates

$$\hat{x}_i = (\delta_{ij} + \alpha_{ij})\, X_j \tag{47}$$

and the subsequent rotation implies

$$x_i = a_{ij}\, \hat{x}_j = a_{ij}(\delta_{jl} + \alpha_{jl})\, X_l \tag{48}$$

The displacement field u_i is then given by

$$u_i = x_i - X_i = (a_{ij}\, \alpha_{jl} + a_{il} - \delta_{il})\, X_l \tag{49}$$

Since the Green strain tensor is

$$E_{ij} = \frac{1}{2}\left(\frac{\partial u_i}{\partial X_j} + \frac{\partial u_j}{\partial X_i} + \frac{\partial u_\iota}{\partial X_i}\frac{\partial u_l}{\partial X_j}\right) \tag{50}$$

it follows from equations (49) and (50) that

$$E_{ij} = \alpha_{ij} + \tfrac{1}{2}\alpha_{li}\, \alpha_{lj} \tag{51}$$

Neglecting the translations, which obviously cause no strains, the rigid body displacements are

$$u_i^{\mathrm{rig}} = (a_{ij} - \delta_{ij})\, X_j \tag{52}$$

and from equations (49) and (52) it follows that

$$u_i^{\mathrm{def}} = u_i - u_i^{\mathrm{rig}} = a_{ij}\, \alpha_{jl}\, X_l \tag{53}$$

Since the components of the displacement vector in the convected and global co-ordinates are related by the orthogonal transformation a_{ij}

$$\hat{u}_i^{\mathrm{def}} = a_{ji}\, u_j^{\mathrm{def}} = \alpha_{il}\, X_l \tag{54}$$

Using equations (47) and (54), we find

$$\hat{u}_i^{\mathrm{def}} = \alpha_{il}(\delta_{lj} + \alpha_{lj})^{-1}\, \hat{x}_j \tag{55}$$

As α_{ij} are assumed small

$$(\delta_{lj} + \alpha_{lj})^{-1} = \delta_{lj} - \alpha_{lj} + \alpha_{lk}\, \alpha_{kj} + O^3(\alpha_{lj}) \tag{56}$$

so that

$$\hat{u}_i^{\mathrm{def}} = [\alpha_{il} + O^2(\alpha_{il})]\, \hat{x}_l \tag{57}$$

If we define the convected strains by

$$\hat{\varepsilon}_{ij} = \frac{1}{2}\left(\frac{\partial \hat{u}_i^{\mathrm{def}}}{\partial \hat{x}_j} + \frac{\partial \hat{u}_j^{\mathrm{def}}}{\partial \hat{x}_i}\right) \tag{58}$$

it follows that

$$\hat{\varepsilon}_{ij} = \alpha_{ij} + O^2(\alpha_{ij}) \tag{59}$$

Therefore, for small α_{ij}, $\hat{\varepsilon}_{ij}$ measure the pure deformation and agree in first-order terms with the Green strain tensor as given by equation (51).

A second question regarding this formulation is its relationship to previous formulations, in particular, the role of the initial stresses. The initial stress does not appear explicitly in equation (11) because the variational principle presented here is a total variational principle rather than

an incremental variational principle, so it must always be applied relative to an undeformed, unstressed configuration. However, this does not mean that the role of the initial stresses which appear in intermediate configurations are neglected. If this variational form is applied to obtain relations between incremental nodal forces and displacements, the initial stresses appear in the usual manner.

Consider two configurations, denoted by superscripts I and $I+1$. From equation (11), it follows that

$$\{f^{I+1}\} = [T^{I+1}]^{\mathrm{T}} \int_V [\mathbf{E}]^{\mathrm{T}} \{\hat{\sigma}^{I+1}\} \tag{60}$$

$$\{f^{I}\} = [T^{I}]^{\mathrm{T}} \int_V [\mathbf{E}]^{\mathrm{T}} \{\hat{\sigma}^{I}\} \tag{61}$$

Hence

$$\begin{aligned} \{\Delta f\} &= [T^{I+1}]^{\mathrm{T}} \int_V [\mathbf{E}]^{\mathrm{T}} \{\hat{\sigma}^{I+1}\} - [T^{I}]^{\mathrm{T}} \int_V [\mathbf{E}]^{\mathrm{T}} \{\hat{\sigma}^{I}\} \\ &= [T^{I}]^{\mathrm{T}} \int_V [\mathbf{E}]^{\mathrm{T}} \{\Delta \hat{\sigma}\} + [\Delta T]^{\mathrm{T}} \int_V [\mathbf{E}]^{\mathrm{T}} \{\hat{\sigma}^{I+1}\} \end{aligned} \tag{62}$$

The first right-hand term of equation (62) results in the usual linearized tangential stiffness matrix, while the second term results in the initial stress stiffness. Since an explicit temporal integration is used in this paper, the relations between incremental forces and displacements are not needed.

REFERENCES

1. J. A. Stricklin, W. E. Haisler and W. A. von Riesemann, 'Computation and solution procedure for nonlinear analysis by combined finite element–finite difference methods', *Natl Symp. Computerized Struct. Anal. and Design*, George Washington Univ., Washington, D.C., 1972.
2. S. W. Key and Z. E. Beisinger, 'The transient dynamic analysis of thin shells by the finite element method', *3rd Conf. Matrix Methods Struct. Mech.*, Wright–Patterson Air Force Base, Ohio, 1971.
3. R. D. Krieg and S. W. Key, 'Transient shell response by numerical time integration', *2nd U.S.–Japan Seminar Matrix Methods in Struct. Anal.*, Berkeley, Calif., 1972.
4. C. J. Costantino, 'Finite element approach to stress wave problems', *J. Eng. Mech. Div., ASCE*, **93**, 153–166 (1967).
5. C. J. Costantino, *Stress Waves in Layered Arbitrary Media—SLAM Code Free Field Study*, **1–4**, SAMSO Report TR–68–181, IITRI, Chicago, Ill., 1968.
6. R. H. Gallagher, J. Padlog and P. P. Bijlaard, 'Stress analysis of heated complex shapes', *J. Am. Rocket Soc.* **32**, 700–707 (1962).
7. M. Dibaj and J. Penzien, 'Nonlinear seismic response of earth strucutres', *Report* for State of Calif., Dept., of Water Res., No. 352984, Univ. of Calif. at Berkeley, Calif., 1969.
8. I. Farhoomand and E. L. Wilson, 'A nonlinear finite element code for analyzing the blast response of underground structures', *Contract Report* for Defense Atomic Support Agency, W–70–1, Univ. of Calif. at Berkeley, Calif., 1970.
9. J. T. Oden, 'Finite element applications in linear and nonlinear thermo-viscoelasticity', *EMD Specialty., Conf., ASCE*, 32–35, Raleigh, N.C., 1967.
10. J. T. Oden, *Finite Elements of Nonlinear Continua*, McGraw-Hill, New York, 1972.
11. D. W. Malone and J. J. Connors, 'Finite elements and dynamic viscoelasticity', *J. Eng. Mech. Div., ASCE*, **97**, 1145–1158 (1971).
12. E. H. Wu and E. A. Witmer, 'Finite element analysis of large elastic–plastic transient deformations of simple structures', *AIAA J.* **9**, 1719–1724 (1971).
13. M. Harztman and J. R. Hutchinson, 'Nonlinear dynamics of solids by the finite element methods', *Comput. Struct.* **2**, 47–77 (1972).
14. J. F. McNamara and P. V. Marcal, 'Incremental stiffness method for finite element analysis of the nonlinear dynamic problem', *Proc. Int. Symp. Numerical and Computer Methods in Struct. Mech.*, Urbana, Ill., 1971.

15. J. H. Argyris, S. Kelsey and H. Kamel, 'Matrix methods of structural analysis: a précis of recent developments', in *Matrix Methods of Structural Analysis* (Ed. B. F. deVenbeke), AGARDograph 72, Pergamon Press, New York, 1964.
16. G. A. Wempner, 'Finite elements, finite rotations and small strains of flexible shells', *Int. J. Solids Struct.* **5**, 117–153 (1969).
17. D. W. Murray and E. L. Wilson, 'Finite element large deflection analysis of plates', *J. Eng. Mech. Div., ASCE*, **95**, 143–165 (1969).
18. H. S. Levin, H. Armen, R. Winter and A. Pifko, 'Nonlinear behavior of shells of revolution under cyclic loading', *Natl Symp. Computerized Struct. Anal. and Design*, George Washington Univ., Washington, D.C., 1972.
19. R. H. Gallagher, 'Geometrically nonlinear finite element analysis', *Spec. Conf. Finite Element Method in Civil Engineering*, McGill University, Montreal, 1972.
20. M. A. Biot, *Mechanics of Incremental Deformations*, Wiley, New York, 1965.
21. H. A. Balmer and E. A. Witmer, 'Theoretical–experimental correlation of large dynamic and permanent deformation of impulsively loaded simple structures', *Report*, FDL–TDR–64–108, Air Force Flight Dyn. Lab., Wright–Patterson Air Force Base, Ohio, 1964.